Effect of Crystallization Methods on Morphology and Photocatalytic Activity of Anodized TiO_2 Nanotube Array Films

Jiaguo Yu,* Gaopeng Dai, and Bei Cheng

State Key Laboratory of Advanced Technology for Materials Synthesis and Processing, Wuhan University of Technology, Wuhan 430070, People's Republic of China

Received: July 8, 2010; Revised Manuscript Received: September 30, 2010

Highly ordered TiO_2 nanotube array (TNs) thin films were prepared by electrochemical anodization of titanium foil in a mixed electrolyte solution containing Na_2SO_4, H_3PO_4, NaF, and sodium citrate and then treated by calcination, vapor-thermal, and hydrothermal methods, respectively. The as-prepared samples were characterized by X-ray diffraction, scanning electron microscopy, transmission electron microscopy, and X-ray photoelectron spectroscopy. The photocatalytic activity of the film samples was evaluated by photocatalytic degradation of methyl orange (MO) aqueous solution under UV light irradiation. The production of hydroxyl radicals ($^{\bullet}OH$) on the surface of UV-irradiated samples was detected by a photoluminescence technique using terephthalic acid as a probe molecule. The transient photocurrent response was measured by several on−off cycles of intermittent irradiation. It was found that post-treatment exhibited a great influence on the morphology, crystallization, and photocatalytic activity of TNs thin films. Calcination and vapor-thermal treatment had no great influence on surface morphology and architecture of the TNs films. On the contrary, for the hydrothermal treated samples, the nanotube array structures were completely destroyed, and only aggregated anatase particles were observed. The vapor-thermal-treated films showed higher photocatalytic activity than the calcined and hydrothermal treated films. This was attributed to the fact that the vapor-thermal-treated films had better crystallization than the calcined films and remained tubular structures compared with the hydrothermal-treated samples. Good crystallization and remaining tubular structures resulted in the highest photocatalytic activity of the vapor-thermal-treated films.

1. Introduction

In recent years, titanium dioxide as one of the most important multifunctional metal oxides has been extensively investigated for its wide applications in environmental purification and solar energy conversion.[1−15] Among various oxide semiconductor photocatalysts, titania has proved to be a very important photocatalyst because of its strong oxidizing power, nontoxicity, and long-term photostability. To avoid the use of powder photocatalyst, which has to be separated from a slurry system after photocatalytic reaction, TiO_2 thin film photocatalysts have been prepared on various substrates.[16−18] There are various methods for the preparation of TiO_2 thin films such as vacuum evaporation, sputtering, chemical vapor deposition (CVD), sol−gel, and liquid-phase deposition (LPD) methods.[19] However, these methods have some limitations for industry applications. For example, vacuum evaporation, sputtering, and CVD methods require special and expensive apparatuses for the deposition of films. The sol−gel method requires coating repeatedly in order to get thick films. The LPD method requires special raw material; also, experimental conditions are difficult to be controlled.[19−23] Since Zwilling et al. for the first time reported the fabrication of highly ordered TiO_2 nanotube arrays (TNs) thin films by anodization of titanium foil in a HF-containing electrolyte in 1999.[24a] The investigations on the anodized TNs thin films have attracted considerable attention.[24−37] Also, the dimensions of TiO_2 nanotubes can be precisely controlled. Uniform TiO_2 nanotubes of various pore sizes (22−110 nm), lengths (200−1 000 000 nm), and wall thicknesses (7−34 nm) are easily obtained by controlling electrochemical conditions. Considering their large specific surface area, high pore volume, and novel morphology, the obtained NTs films will offer new chances to design various 1D TiO_2-related functional materials by doping, deposition, and sensitization.[32,37]

Many investigations have indicated that the photocatalytic activity of TiO_2 thin films is highly related to the conditions of preparation and methods of post-treatment. Especially, post-treatment methods have exhibited a significant influence on the photocatalytic activity of TiO_2 thin films.[16,17,38] For example, the photocatalytic activity of mesoporous and ordinary TiO_2 thin films could be significantly enhanced by surface acid treatment.[16,38] Furthermore, we reported effects of trifluoroacetic acid modification on the surface microstructures and photocatalytic activity of mesoporous TiO_2 thin films.[39] Very recently, we reported the effect of calcination temperature on morphology and photoelectrochemical properties of anodized titanium dioxide nanotube arrays films.[40] Our results indicated that low temperatures (below 600 °C) had no great influence on surface morphology and architecture of the TNs sample. At 800 °C, the nanotube arrays are completely destroyed and only dense rutile crystallites are observed. At 600 °C, the sample shows the highest photocatalytic activity due to its biphase composition, good crystallization and remaining tubular structures.[40] However, the investigation of Macak et al. indicated that the 450 °C calcined TiO_2 NTs show better photocatalytic activity than the amorphous as well as other calcined temperatures.[30] This probably is due to the difference of photocatalytic experimental conditions and preparation method of TiO_2 NTs.[30,40] Therefore,

* To whom correspondence should be addressed. Phone: 0086-27-87871029. Fax: 0086-27-87879468. E-mail: jiaguoyu@yahoo.com.

10.1021/jp106324x
Published on Web 10/22/2010

TABLE 1: Experimental Conditions for the Preparation of Samples and Their Phase Structures, Average Crystallite Size and Relative Crystallinity

samples	treatment methods	experiment conditions	phase[a]	crystallite size (nm)	relative crystallinity[b]
TNs-As	as-prepared		Am		
TNs-Ca	calcination	450°C,3h	A	20.5	1
TNs-Va	vapor-thermal	180°C,2h	A	24.5	1.4
TNs-Hy	hydrothermal	180°C,2h	A	28.9	1.7

[a] Am and A denote amorphous and anatase, respectively. [b] Relative anatase crystallinity: the relative intensity of the diffraction peak from the anatase (101) plane (reference = TNs-Ca).

it is strongly necessary to further elucidate the influence of different post-treatment methods on the photocatalytic activity and surface microstructures of TNs films. However, to our knowledge, there are no studies performed on the effects of vapor and hydrothermal treatment on the morphology and photocatalytic activity of the TNs films. In this work, we prepared highly ordered TNs thin films on a titanium foil in a containing-fluoride mixed electrolyte solution. The prepared TNs films were crystallized by calcination, vapor-thermal and hydrothermal methods, respectively. The effects of three treatment methods on the morphology, structures, crystallization, photocatalytic activity, and photoelectrochemical properties of TNs samples were investigated and discussed. This is the first report on the comparative studies of photocatalytic activity of TNs thin films treated by calcination, vapor-thermal, and hydrothermal methods. This investigation will provide new insights into preparation of highly photocatalytic activity TiO_2 thin films.

2. Experimental Section

2.1. Preparation of TiO_2 Nanotube Array Films. All chemicals used in this study were analytical grade and were purchased from Shanghai Chemical Regent Factory of China without further treatment. Distilled water was used in all experiments. The self-organized TiO_2 nanotube arrays were grown by anodization of Ti foils in an aqueous solution containing 0.5 M Na_2SO_4, 0.5 M H_3PO_4, 0.2 M $C_6H_5Na_3O_7$ (sodium citrate), and 0.5 wt % NaF solution at pH ca. 4, similar to the method described by Kang et al.[41] Prior to anodization, Ti foils (0.25 mm in thickness, 99% purity) were degreased by sonicating in acetone, isopropanol, and methanol, rinsed with distilled water and dried in a nitrogen stream. Anodization was performed in a two-electrode configuration connected to a DC power supply (RXN-602D, Shenzhen Zhaoxin Electronic Equipment and Instruments Co., China) using titanium foil as the working electrode and platinum foil as the counter electrode under a constant 20 V anodic potential for 10 h at room temperature. After anodic oxidation, the samples were rinsed with distilled water and dried in a N_2 stream. The crystallization treatment of as-prepared TiO_2 nanotube array films was performed by the calcination, vapor-thermal and hydrothermal methods, and the obtained samples were labeled as TNs-Ca, TNs-Va, and TNs-Hy, respectively. The detailed experimental conditions for the preparation of samples were listed in Table 1 and as follows.

(1) The as-prepared TiO_2 nanotube array film was calcined at 450 °C in air for 3 h at heating and cooling rates of 2 °C/min.

(2) 2 × 2 cm^2 as-prepared TiO_2 nanotube array film was placed on the support to avoid direct contact with the water, which was then placed into a 100-mL stainless steel autoclave with a 100 mL Teflon linear. Two mL distilled water was added into the linear. The autoclave was sealed and kept at 180 °C for 2 h and cooled to room temperature naturally. The sample was taken out and dried at 60 °C for 6 h.

(3) 2 × 2 cm^2 as-prepared TiO_2 nanotube array films was placed into a 100-mL Teflon-lined autoclave, which was then filled with water up to 80% of the total volume. The autoclave was sealed and kept at 180 °C for 2 h and then cooled to room temperature naturally. The sample was taken out and dried at 60 °C for 6 h.

2.2. Characterization. The morphology observation was carried out by an S-4800 field emission scanning electron microscope (SEM, Hitachi, Japan), which was linked with an Oxford Instruments X-ray analysis system, at an accelerating voltage of 10 kV. Transmission electron microscopy (TEM) analyses were conducted by a JEM-2100F electron microscope (JEOL, Japan), using a 200-kV accelerating voltage. X-ray diffraction (XRD) patterns, obtained on a D/MAX-RB X-ray diffractometer (Rigaku, Japan) using Cu Kα radiation at a scan rate (2θ) of 0.05° s^{-1}, were used to characterize the identity of any phase present and their crystallite size. The accelerating voltage and applied current were 40 kV and 80 mA, respectively. The average crystallite size of anatase phase was quantitatively calculated using Scherrer formula ($d = 0.9\lambda/B \cos\theta$, where d, λ, B, and θ are crystallite size, Cu Kα wavelength (0.15418 nm), full width at half-maximum intensity (fwhm) of (101) for anatase peak in radians, and Bragg's diffraction angle, respectively) after correcting the instrumental broadening. X-ray photoelectron spectroscopy (XPS) measurements were done on a VG ESCALAB MKII XPS system with Mg Kα (1253.6 eV) source and a charge neutralizer. All the binding energies were referenced to the C1s peak at 284.8 eV of the surface adventitious carbon.

2.3. Measurement of Photocatalytic Activity. The photocatalytic activity of the samples was evaluated by the photocatalytic decolorization of methyl orange (MO, a kind of chemically stable and persistent nitrogen-containing dye pollutant) in water at ambient temperature.[19] Experiment was as follows: TNs sample (2 × 2 cm^2) was placed into 5 mL of MO aqueous solution (4 × 10^{-5} M) in a 25-mL beaker. Before photocatalytic reaction, the solution was allowed to reach an adsorption−desorption equilibrium among the photocatalyst, MO, and water. A 300-W xenon lamp (Changtuo, China) positioned above 10 cm away from the beaker was used as a light source to trigger the photocatalytic reaction. One face of the TNs samples was irradiated along the normal direction. The average light intensity striking on the surface of the reaction solution was about 20 mW cm^{-2}, measured by a UV meter (the photoelectric instrument factory of Beijing Normal University, China) with the peak intensity of 365 nm. The concentration of MO was determined by an UV−visible spectrophotometer (UV-2550, Shimadzu, Japan). After UV light irradiation for every 10 min, the reaction solution was taken out to measure the concentration change of MO. As for the MO aqueous solution with low concentration, its photocatalytic decolorization was a pseudofirst-order reaction and its kinetics was expressed as $\ln(C_0/C) = kt$, where k is the apparent rate constant and C_0 and C are the initial and reaction concentrations of MO in water, respectively.[19]

2.4. Analysis of Hydroxyl Radicals (•OH). Hydroxyl radicals (•OH) produced on the surface of photoilluminated TiO_2 was detected by the photoluminescence (PL) technique using terephthalic acid as a probe molecule, which readily reacted with •OH to produce highly fluorescent product, 2-hydroxyterephthalic acid. The method relied on the PL signal at 425

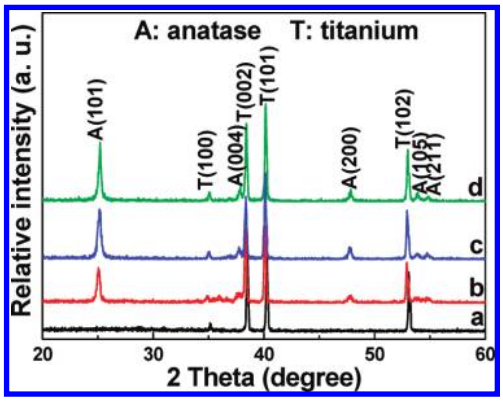

Figure 1. XRD patterns of the TNs samples before and after treatment. (a) Untreated, (b) calcination, (c) vapor-thermal, and (d) hydrothermal.

nm of 2-hydroxyterephthalic acid. The PL intensity of 2-hydroxyterephtalic acid was proportional to the amount of •OH radicals produced on the surface of TiO_2.[42−44] Experimental procedures are similar to the measurement of photocatalytic activity except that MO aqueous solution was replaced by the 5×10^{-4} M TA aqueous solution with a concentration of 2×10^{-3} M NaOH solution. PL spectra of generated 2-hydroxyterephthalic acid were measured by a Hitachi F-7000 fluorescence spectrophotometer (Hitachi, Japan). After light irradiation for every 10 min, the reaction solution was used to measure the increase of the PL intensity at 425 nm excited by 315 nm light.

2.5. Photoelectrochemical Measurements. Photocurrents were measured by an electrochemical analyzer (CHI660C Instruments, CHI, China) in a standard three-electrode system using the prepared samples as the working electrodes with an active area of ca. 0.5 cm^2, a Pt wire as the counter electrode, and Ag/AgCl (saturates KCl) as a reference electrode. A 300-W Xe arc lamp was used as an UV light source, and the light intensity was about 20 mW/cm^2. A 1 M Na_2SO_4 aqueous solution was used as the electrolyte.[37]

3. Results and Discussions

3.1. Crystal Structure. It is well-known that the phase structure, crystallite size, and crystallinity of TiO_2 are of great influence on its photocatalytic activity and photoelectrochemical properties.[40] Therefore, XRD was used to characterize the changes of phase structures and crystallite sizes of the prepared TNs samples before and after post-treatment. Figure 1 shows effects of three crystallization methods on phase structures of the TNs samples. For the as-prepared (or untreated) TNs samples (see Figure 1a), all the diffraction peaks are indexed to metal titanium phase (JCPDS 44−1294, $a = 2.951$ Å, $c = 4.683$ Å, space group *P*63/*mmc* (194)), and no peaks of any TiO_2 phases (anatase, rutile or brookite) are observed, implying that the as-prepared TNs films are an amorphous phase before post-treatment. For three treated samples, except the diffraction peaks of Ti substrate, two obvious peaks at $2\theta = 25.3$ and 48.1°, respectively, corresponding to (101) and (200) plane diffraction of anatase TiO_2 (JCPDS No. 21−1272, $a = 3.7852$ Å, $c = 9.5139$ Å, space group: $I4_1/amd$ (141)) are clearly observed (parts b−d of Figure 1). Further observation indicates that post-treatment methods greatly influence on the crystallization of the TNs samples. For the hydrothermal-treated sample, XRD peak intensities of anatase are strongest and the width of XRD diffraction peaks of anatase is narrowest, indicating the formation of greatest TiO_2 crystallites and enhancement of crystallization. The crystallinity of TiO_2 was quantitatively evaluated by comparing the relative intensity of the anatase (101) diffraction peak. Table 1 lists the average crystalline sizes and relative anatase crystallinity of TNs samples obtained by three treatment methods. It can be seen that after hydrothermal treatment, the TiO_2 film has the largest average crystalline size and the strongest relative anatase crystallinity. On the contrary, after calcination, the TiO_2 film has the smallest crystalline size and the weakest relative anatase crystallinity, indicating that vapor-thermal and hydrothermal treatments are more efficient methods for the preparation of highly crystallized TiO_2 thin films at a low temperature. This also suggests that water molecules can enhance the phase transformation of amorphous to anatase and the growth of anatase crystallite possibly as a phase transformation catalyst. Therefore, it is not surprising that the phase transformation of amorphous to anatase can occur at a 180 °C low temperature due to the presence of H_2O.[45,46] Of course, the existence of pressure (for vapor-thermal and hydrothermal methods) is also beneficial to the occurrence of the amorphous to anatase phase transition.[47]

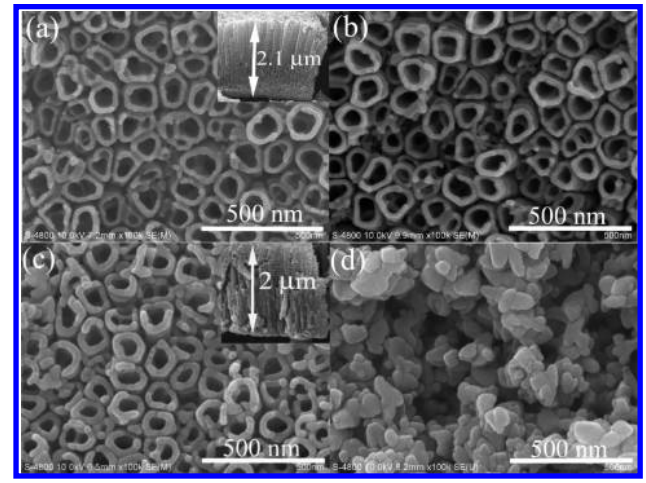

Figure 2. SEM images of the TNs samples before and after treatment. (a) Untreated, (b) calcination, (c) vapor-thermal, and (d) hydrothermal. The insets in (a) and (c) show the cross-sectional SEM images of untreated and vapor-treated TN samples, respectively.

3.2. SEM Studies. The self-organized TiO_2 nanotube arrays were fabricated by anodic oxidation of Ti foils and then crystallized by three different treatment methods (see experimental section). The morphology changes of the TNs samples were observed by SEM. Figure 2a shows a typical SEM image of the untreated TNs. Highly ordered nanotube arrays grown on a Ti substrate are observed, which have an average pore diameter of around 110 nm and wall thickness of ca. 20 nm. The inset in Figure 2a exhibits a cross-sectional SEM image of the TNs, indicating that the TNs contain well-aligned nanotubes of about 2.1 μm in length which grow vertically from a Ti substrate. The chemical composition of the TNs was determined by energy dispersive X-ray spectroscopy (EDX) experiments. EDX results (not shown here) demonstrate that the as-prepared TNs samples contain Ti, O, and a small amount of F element, confirming TNs being TiO_2. F element is from the precursor NaF due to surface adsorption.[48] Post-treatment methods have a great influence on the morphology of TNs. It can be seen from Figure 2b that the 450 °C calcined TNs samples still keep their original morphology, and the pore diameter and wall thickness of the nanotubes have no obvious change, indicating that low-temperature calcination has no influence on the surface morphology and architecture of the TNs samples. This is in agreement with our recent report.[40] For the 180 °C vapor-thermal

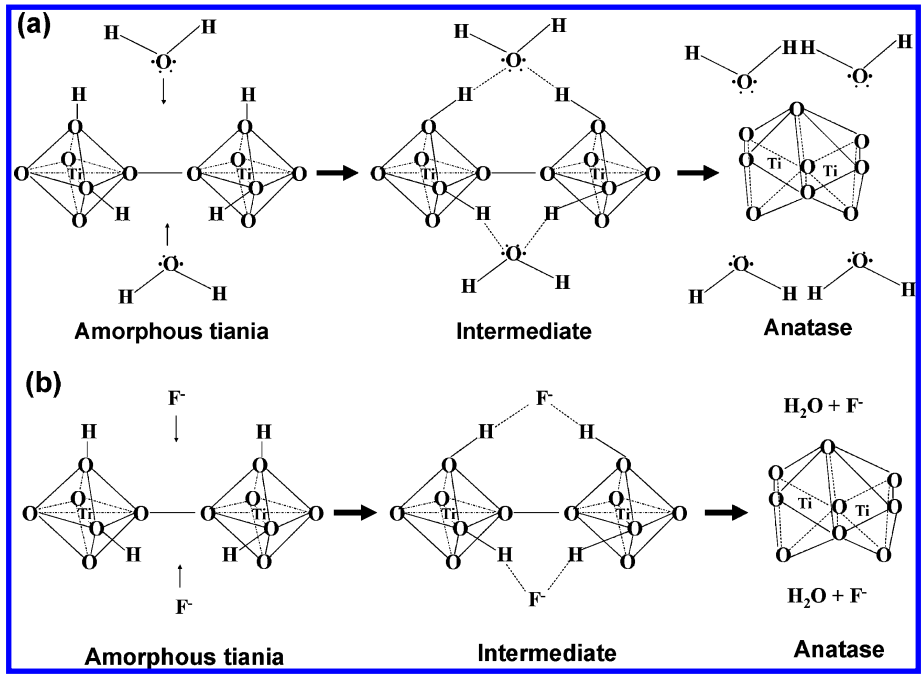

Figure 3. Schematic diagram of hydrothermal reaction mechanism of the amorphous-to-anatase phase transformation (a) in pure water and (b) in the presence of F^-.

treated samples, the surface morphology of the TNs sample has an obvious change (Figure 2c). The thickness of nanotube wall increases (from 20 to 30 nm) and the inner diameter of nanotube decreases (from 70 to 50 nm). Surprisingly, when the TNs films were hydrothermal treated at 180 °C for 2 h, the surface morphology of the TNs films has a great change (Figure 2d). The nanotube array structures are completely destroyed and only TiO_2 aggregated particles with size of ca. 100−150 nm are observed (Figure 2d), indicating the collapse of the tubular structure and formation of TiO_2 aggregated particles.

3.3. Mechanism of Crystallization and Morphology Evolution. It is well-known that anatase TiO_2 with a high surface area and good crystallization is desirable to enhance the photocatalytic activity, since such anatase TiO_2 have relatively few defects in its crystal structure. These properties are, of course, difficult to be achieved at the same time. The above XRD and SEM results demonstrate that the existence of water has a strong influence on the crystallization and morphology of amorphous TNs. In three crystallization cases, anatase polymorph was produced, with no rutile present. The calcined TNs sample exhibited less crystallinity than the TNs sample treated by either vapor or hydrothermal methods. Therefore, the presence of water in the reaction system catalyzes the crystallization step. This is in agreement with the results previously published for anatase crystallized from amorphous titania in a hydrothermal environment.[49,50]

Why can water molecules catalyze the crystallization reaction of amorphous TiO_2? This is due to the fact that the presence of water in the crystallization reaction catalyzes the rearrangement of the TiO_6 octahedra in the amorphous titania by adsorption to the amorphous titania surface, increasing the rate of crystallization dramatically. Figure 3 schematically shows the reaction mechanism for hydrothermal crystallization of anatase. For anatase, under hydrothermal conditions, the rearrangement of these TiO_6 octahedra from amorphous TiO_2 is performed by a dehydration reaction. First, water molecules form bridges between surface OH groups of two different octahedra by sharing only one common vertex, using the two lone pairs of electrons on the oxygen (Figure 3a). Then, the bridges link two octahedra by sharing a triangular face and, meanwhile, align the octahedra correctly. Finally, a dehydration occurs, and the four water molecules are lost, resulting in the two titanium ions linked by two further oxygen ion vertexes, and thus sharing a face (anatase).[50] Our previous and present results indicate that the presence of a small amount of F^- increases the rate of this reaction and the crystallization of anatase TiO_2. The observed effect of the fluoride ion in increasing the crystallization rate under hydrothermal conditions can also be explained according to bridge formation by coordination to the F^- ion when it is in low concentrations (Figure 3b). Therefore, it is not surprising that the hydrothermal-treated TNs sample shows the best crystallization due to the presence of water molecules and F^-. Why the three treated TNs samples show a significant difference in morphology? This is related to three different crystallization mechanisms. For the 450 °C calcined TN sample, its morphology has no obvious change. This is due to the fact that the in situ solid-state phase transformation from amorphous to anatase caused by calcination has no influence on morphology. For the 180 °C hydrothermal-treated TN sample, its phase transformation and crystallization mechanism is the dissolution recrystallization mechanism. We propose a model to explain the amorphous-to-anatase phase transformation and morphology architecture evolution of TNs samples during hydrothermal treatment, which is schematically shown in Figure 4A. The nucleation and growth of anatase phase most probably first occur at the interface between TiO_2 nanotubes and Ti substrate due to the fact that the interface nucleation (IN) of anatase has the lowest activation energy of nucleation.[51] Then, these anatase crystallites grow in size with increasing hydrothermal time. However, the amorphous TiO_2 nanotube wall remains out of equilibrium with the surrounding solution and has a strong tendency to dissolve due to its higher solubility and surface energies compared to the as-formed anatase phase. This results in the rapid growth of anatase crystallites, destruction and collapse of tubular architectures, and formation of coarsened anatse aggregated particle film.[52] The corresponding TEM images of titania nanotube arrays prepared at 180 °C for different time further confirm the above proposed morphology transfor-

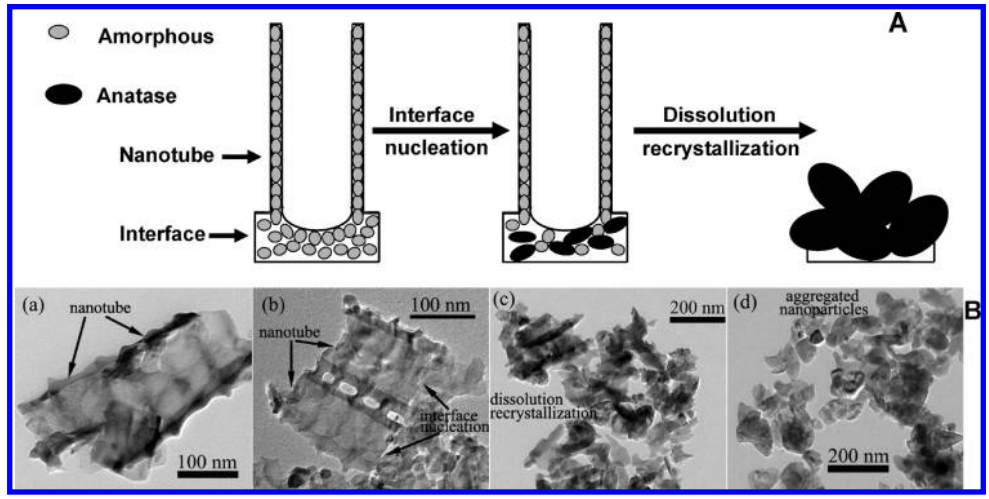

Figure 4. (A) Schematic diagram of the amorphous-to-anatase phase transformation and morphology evolution of the TNs samples treated by hydrothermal method. (B) TEM images of tiania nanotube arrays after hydrothermal treatment at 180 °C for (a) 0 min, (b) 15 min, (c) 30 min, and (d) 2 h.

mation mechanism (see Figure 4B). For the 180 °C vapor-treated TN sample, its crystallization is first performed by a solid-state phase transformation and then epitaxial crystal growth mechanism. Therefore, the thickness of nanotube wall becomes thick.

3.4. XPS Studies. XPS was used to investigate the change of the surface compositions and chemical status of the TiO_2 films before and after post-treatments. Figure 5A shows the comparison of survey spectra of the TiO_2 films before and after post-treatments. Sharp photoelectron peaks appear at binding energies of 458 (Ti 2p) and 531 eV (O 1s) in four cases, along with a C 1s peak at 285 eV due to contamination from the XPS instrument itself. As expected, an additional peak at 684 eV (F 1s) is found in the survey spectrum of the as-prepared TNs sample. The F 1s binding energy peak (Figure 5B) originates from surface fluoride (≡Ti—F) formed by ligand exchange between F^- and surface hydroxyl groups. No signal for F^- in the lattice of TiO_2 (binding energy = 688.5 eV) is found.[14,52−54] This indicates that surface fluorination of TiO_2 readily takes place in an acidic hydrothermal environment (pH 1−4), as reported in other systems.[53] The relative atomic ratios of the detected elements are shown in Table 2. The maximum F content (about 6.9 at %) was found in the as-prepared TN sample due to its amorphous phase structure and surface fluorination.[48,53a] The results of Albu et al. also indicated that the fluoride content in amorphous nanotubes is much higher than the annealed tube as the outer shell of TiO_2 nanotubes contains the fluoride-rich layer.[53a] Therefore, it is not surprising that the F contents in the vapor and hydrothermal treated TNs films decrease. Also, the hydrothermal-treated TNs sample contains less F element, suggesting that the absorbed F^- is desorbed and dissolves in water during hydrothermal treatment. However, almost no F element is found for 450 °C calcined TN film due to the evaporation of the F element at high temperature.[40] Figure 5B shows the comparison of high-resolution XPS spectra of the F 1s region of TNs films before and after post-treatments. The peak at 684.4 eV is assigned to F^- ions physically absorbed on the surface of TiO_2. Figure 4C shows the high-resolution XPS spectra of the O1s region, taken on the surface of TNs films before and after post-treatments. The O1s region can be fitted into two contributions. The main peak at 530.2 eV is attributed to Ti−O in TiO_2, and the other minor peak at 531.6 eV is ascribed to the OH on the surface of TiO_2.[16] Table 3 shows the curve fitting of the XPS spectra for the O1s region of the samples. Although some H_2O is easily adsorbed on the surface of TNs films during the vapor and hydrothermal treatment, the physically absorbed H_2O on the TiO_2 is easily desorbed under the ultrahigh vacuum condition of the XPS system. Therefore, the hydroxyl on the surface can be attributed to the Ti−OH on the surface of TiO_2 films. Further observation indicates that the hydroxyl content of the calcined TNs sample is the lowest. This is due to a dehydration reaction (Ti−OH + HO−Ti → Ti−O−Ti + H_2O) occurring on the surface of the calcined TNs films. Contrarily, there is an obvious increase in hydroxyl content for the vapor and hydrothermal treated samples. This is due to the fact that the F^- on the surface of TNs films was replaced by OH, resulting in the increase in OH content.

3.5. Photocatalytic Activity. The photocatalytic activity of the TNs films was evaluated by photocatalytic degradation decolorization of MO aqueous solution under UV light irradiation. Figure 6 shows the comparison of photocatalytic activities of the untreated and treated samples. The as-prepared TNs sample exhibits negligible activity (rate constant, 0.003 min^{-1}) due to its amorphous structure.[40] For vapor-treated TN samples, the highest photocatalytic activity is observed with a rate constant of 0.047 min^{-1} (see Figure 6A); MO was almost completely degraded within 1 h (see Figure 6B). The highest photocatalytic activity is partly due to its large specific surface area and high anatase crystalline. It is widely regarded that an anatase TiO_2 with a high surface area, but also a high degree of crystallinity, with a large crystallite size is desirable to enhance the photocatalytic activity. So, because of the high crystallinity, large crystallite size (Table 1), and the specific tubular surface area, it is not surprising that the vapor-treated TNs sample has high photoactivity. Also, highly ordered tubular structures can provide a straight diffusion path for reactant molecules from the solution to the active surface sites and enhance the adsorption efficiency of light.[40] Furthermore, more surface hydroxyl can also enhance the photocatalytic activity. It has been reported that hydroxyl groups on the surface of TiO_2 could react with photogenerated holes ($h^+ + OH^- \rightarrow {}^{\bullet}OH$), resulting in more hydroxyl radicals to participate the photocatalytic reaction.[16,17] Therefore, it is not surprising that the vapor-treated sample has the best photocatalytic activity. Although the hydrothermal-treated sample exhibits the best crystallization, a lower photocatalytic activity is observed comparing with the calcined and vapor-treated samples. This is due to the collapse of tubular structures. Further observation indicates that the 600 °C calcined sample shows better photo-

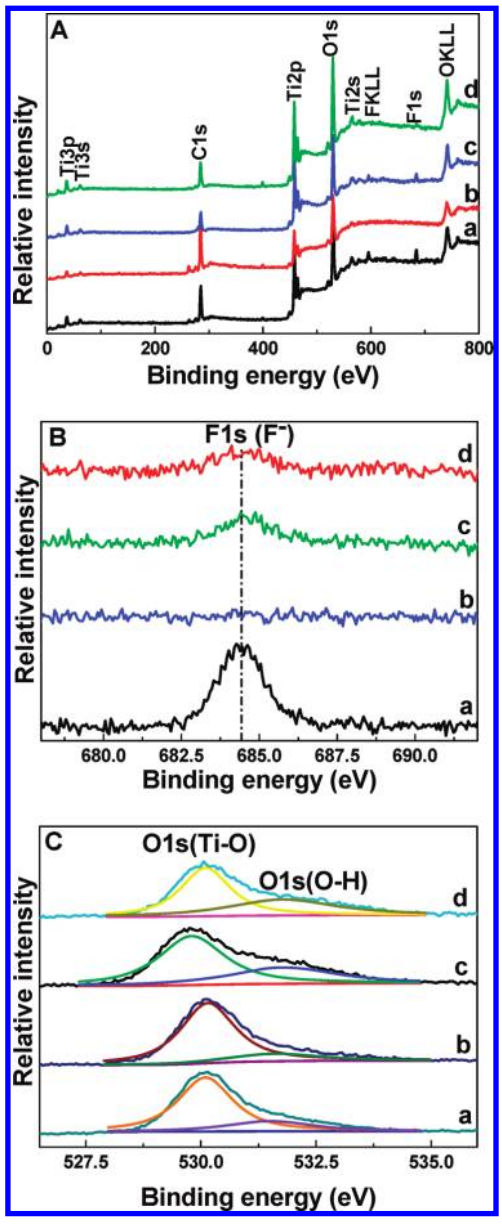

Figure 5. XPS survey spectra (A), high-resolution XPS spectra of F 1s region (B), and O 1s region (C) for the TNs samples before and after treatment. (a) Untreated, (b) calcination, (c) vapor-thermal, and (d) hydrothermal.

TABLE 2: Relative Atomic Percentage of the Samples Determined by XPS

samples	Ti%	O%	F%
TNs-As	28.2	64.9	6.9
TNs-Ca	32.5	67.5	0
TNs-Va	22.5	76.0	1.5
TNs-Hy	24.2	75.2	0.6

catalytic activity than the 450 °C calcined sample due to its biphase structure (80% anatase and 20% rutile) and better crystallization (relative anatase crystallinity: 1.28) but still slightly lower than vapor-treated samples.

3.6. Hydroxyl Radical Analysis. It is well-known that the •OH is assumed to be the major active species responsible for the photocatalytic oxidative reactions. To further confirm the difference of photocatalytic activity of the prepared samples, the hydroxyl radicals produced at UV-illuminated TNs film surface were detected. Figure 7a shows the changes of PL spectra of terephthalic acid solution with irradiation time. A

TABLE 3: Results of Curve Fitting of High-Resolution XPS Spectra for the O1s Region of the Samples

samples		O1s (Ti−O)	O1s (OH)
TNs-As	E_b (eV)	531.1	530.1
	r_i (%)	77.7	22.3
TNs-Ca	E_b (eV)	531.7	530.1
	r_i (%)	83.1	16.9
TNs-Va	E_b (eV)	531.8	529.8
	r_i (%)	72.8	27.2
TNs-Hy	E_b (eV)	531.8	530
	r_i (%)	72.3	27.7

gradual increase in PL intensity at about 425 nm is observed with increasing irradiation time for the vapor-treated sample. However, no PL increase was observed in the absence of UV light or TNs samples. This suggests that the fluorescence is from the chemical reactions between terephthalic acid and •OH produced at the TiO_2/water interface under UV illumination.[42,43] Figure 7b shows the comparison of PL intensity for different samples at 10 min of UV illumination. Usually, PL intensity is proportional to the amount of produced hydroxyl radicals. It can be easily seen that at a fixed time (10 min) the formation rate of OH radicals on the amorphous TNs film is much lower than that of OH radicals on other three anatase-phase TNs films. This is attributed to many imperfections in the amorphous sample to act as recombination sites of photoexcited electron and positive hole.[55] Further observation indicates that the formation rate of OH radicals on the vapor-treated film is the largest. This can be ascribed to the synergetic effects of the several factors including high surface hydroxyl concentration, good anatase crystallinity and remaining tubular structures.

3.7. Transient Photocurrent Response. To further investigate and understand photocatalytic mechanism, the transient

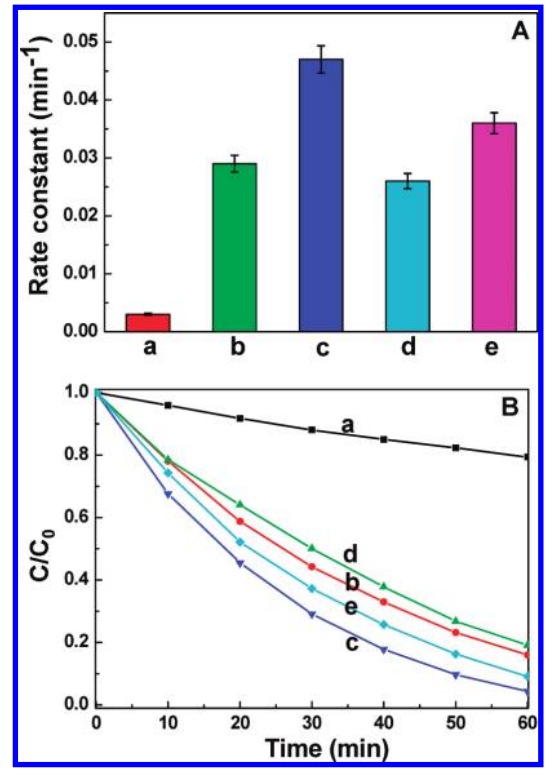

Figure 6. Comparison of photocatalytic activity of the TNs samples before and after treatment for the photocatalytic decomposition of MO in water. (a) Untreated, (b) calcination, (c) vapor-thermal, and (d) hydrothermal. (A) Apparent rate constants. (B) $C/C_0 - t$ curve. C and C_0 denote the reaction and initial concentration of MO in the system, respectively.

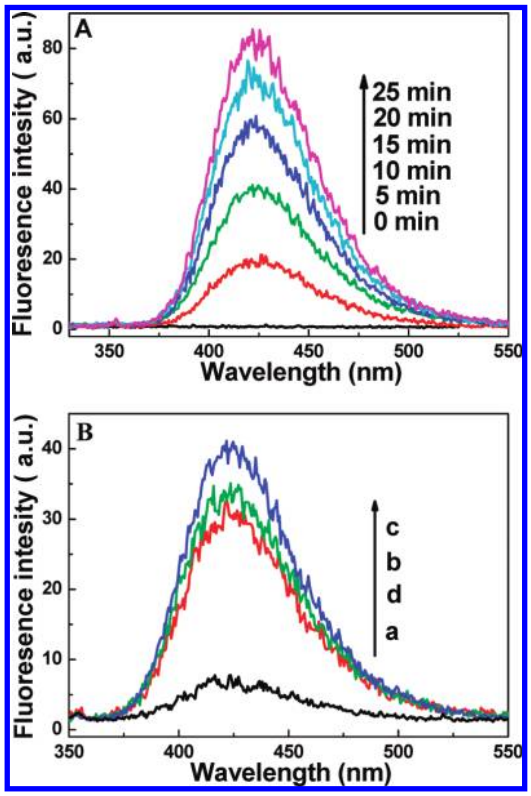

Figure 7. (A) PL spectral changes with UV light irradiation time on the vapor-treated sample in a 5×10^{-4} M basic solution of terephthalic acid. (B) Comparison of PL spectra of the TNs samples before and after treatment in a 5×10^{-4} M basic solution of terephthalic acid under UV light irradiation at a fixed 10 min. (a) Untreated, (b) calcination, (c) vapor-thermal, and (d) hydrothermal.

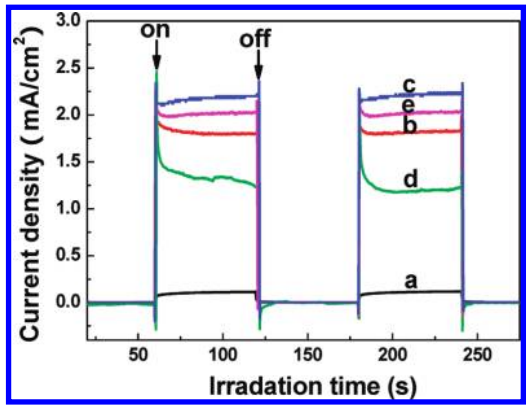

Figure 8. Comparison of transient photocurrent response of the TN samples before and after treatment in a 1 M Na_2SO_4 aqueous solution under UV-light irradiation at 0.5 V vs Ag/AgCl. (a) Untreated, (b) calcination, (c) vapor-thermal, (d) hydrothermal, and (e) 600 °C calcined.

photocurrent responses of the TNs samples before and after crystallization treatment are analyzed by several on−off cycles of intermittent irradiation. Figure 8 shows the comparison of $I-t$ curves of four samples. For all samples, the photocurrent values rapidly decrease to zero as soon as the irradiation of light turns off; meanwhile, the photocurrents again come back to a constant value when the light is again on, which has a good reproducibility. The produced photocurrent is from photogenerated electrons. Under UV light irradiation, the electrons are excited from the valence band to conduction band (O 2p → Ti 3d) of TiO_2 to form photogenerated electron−hole pairs. The photogenerated electrons and holes are rapidly separated under an external potential bias. Then, most photogenerated electrons are transferred to titanium substrate to produce photocurrents. Further observation indicates that post-treatment methods have a great effect on the size of the photocurrent. The untreated TNs sample has least photocurrent due to its amorphous-phase structures. Usually, amorphous TiO_2 contains more defects than crystallized TiO_2, which causes the recombination of photogenerated electrons and holes. So, photogenerated electrons are difficult to transfer to titanium substrate to form photocurrent. However, the vapor-treated TNs sample shows the biggest photocurrent due to its good crystallization and remaining tubular structures. High photocurrent means more photoinduced electrons are transferred effectively from TNs to counter electrode via external circuit, indicating high efficiency of electron−hole pair separation and transfer. For the hydrothermal-treated TNs sample, though it has the best crystallization, its photocurrent is lower than that of the calcined and vapor treated samples due to the collapse of tubular structures. This also implies that the nanotubular microstructures provide an efficient transport channel for photogenerated electrons.[56]

4. Conclusions

In summary, highly ordered TiO_2 nanotube arrays (TNs) are successfully prepared by electrochemical anodization of titanium foil in a mixed electrolyte solution containing Na_2SO_4, H_3PO_4, NaF, and sodium citrate. Post-treatment crystallization methods exhibit a great influence on the crystallinity, morphology, architectures, photocatalytic activity and photoelectrochemical properties of the TiO_2 nanotube array films. A 450 °C low-temperature calcination has no influence on surface morphology and architecture of the TNs sample. Contrarily, the 180 °C hydrothermal treatment exhibits a significant influence on surface morphology and architecture of the TNs sample. The nanotube arrays are completely destroyed, and only anatase aggregated particles are observed. The vapor-treated TNs sample presents highest photocatalytic activity, biggest formation rate of hydroxyl radicals, and photocurrent due to the synergetic effects of the several factors including good crystallization, high surface hydroxyl concentration and remaining tubular structures. The prepared highly ordered TiO_2 nanotube arrays are also of great interest in solar cell, catalysis, separation technology, biomedical engineering, and nanotechnology. This study may provide new insight into the crystallization of TiO_2 photocatalytic materials.

Acknowledgment. This work was partially supported by the National Natural Science Foundation of China (Grant Nos. 50625208, 20773097, 20877061, and 51072154). This work was also financially supported by the National Basic Research Program of China (Grant No. 2007CB613302).

References and Notes

(1) Fujishima, A.; Honda, K. *Nature* **1972**, *238*, 37.
(2) Gratzel, M. *Nature* **2001**, *414*, 338.
(3) Xiang, Q. J.; Yu, J. G.; Cheng, B.; Ong, H. C. *Chem. Asian J.* **2010**, *5*, 1466.
(4) Cheng, Y. W.; Chan, R. C. Y.; Wong, P. K. *Water Res.* **2007**, *41*, 842.
(5) Trapalis, C.; Todorova, N.; Anastasescu, M.; Anastasescu, C.; Stoica, M.; Gartner, M.; Zaharescu, M.; Stoica, T. *Thin Solid Films* **2009**, *517*, 6243.
(6) Ksibi, M.; Rossignol, S.; Tatibouet, J. M.; Trapalis, C. *Mater. Lett.* **2008**, *62*, 4204.
(7) Kim, H.; Choi, W. *Appl. Catal., B* **2007**, *69*, 127.
(8) Yu, J. G.; Xiang, Q. J.; Zhou, M. H. *Appl. Catal., B* **2009**, *90*, 595.
(9) (a) Liu, S. W.; Yu, J. G.; Mann, S. *J. Phys. Chem. C* **2009**, *113*, 10712. (b) Liu, S. W.; Yu, J. G.; Jaroniec, M. *J. Am. Chem. Soc.* **2010**, *132*, 11914.

(10) Li, F. B.; Li, X. Z. *Appl. Catal., A* **2002**, *228*, 15.
(11) (a) Li, Y. X.; Lu, G. X.; Li, S. B. *J. Photochem. Photobiol. A* **2002**, *152*, 219. (b) Jin, Z. L.; Zhang, X. J.; Li, Y. X.; Li, S. B.; Lu, G. X. *Catal. Commun.* **2007**, *8*, 1267. (c) Yu, J. G.; Qi, L. F.; Jaroniec, M. *J. Phys. Chem. C* **2010**, *114*, 13118.
(12) Liu, G.; Wang, L. Z.; Yang, H. G.; Cheng, H. M.; Lu, G. Q. *J. Mater. Chem.* **2010**, *20*, 831.
(13) Xiang, Q. J.; Lv, K. L.; Yu, J. G. *Appl. Catal., B* **2010**, *96*, 557.
(14) Yu, J. G.; Xiang, Q. J.; Ran, J. R.; Mann, S. *CrystEngComm.* **2010**, *12*, 872.
(15) Zhao, L.; Yu, J. G.; Fan, J. J.; Zhai, P. C.; Wang, S. M. *Electrochem. Commun.* **2009**, *11*, 2052.
(16) Yu, J. C.; Yu, J. G.; Zhao, J. C. *Appl. Catal., B* **2002**, *36*, 31.
(17) Yu, J. G.; Zhao, X. J.; Zhao, Q. N. *Mater. Chem. Phys.* **2001**, *69*, 25.
(18) Trapalis, C.; Gartner, A.; Modreanu, M.; Kordas, G.; Anastasescu, A.; Scurtu, R.; Zaharescu, M. *Appl. Surf. Sci.* **2006**, *253*, 367.
(19) Yu, J. G.; Yu, H. G.; Cheng, B.; Zhao, X. J.; Yu, J. C.; Ho, W. K. *J. Phys. Chem. B* **2003**, *107*, 13871.
(20) Yu, J. G.; Xiong, J. F.; Cheng, B.; Liu, S. W. *Appl. Catal., B* **2005**, *60*, 211.
(21) Zhou, M. H.; Yu, J. G.; Liu, S. W.; Zhai, P. C.; Jiang, L. *J. Hazard. Mater.* **2008**, *154*, 1141.
(22) Kato, K.; Tsuzuki, A.; Torii, Y.; Taoda, H.; Kato, T.; Butsugan, Y. *J. Mater. Sci.* **1995**, *30*, 837.
(23) Dijkstra, M. F. J.; Michorius, A.; Buwalda, H.; Panneman, H. J.; Winkelman, J. G. M.; Beenackers, A. A. C. M. *Catal. Today* **2001**, *66*, 487.
(24) (a) Zwilling, V.; Darque-Ceretti, E.; Boutry-Forveille, A.; David, D.; Perrin, M. Y.; Aucouturier, M. *Surf. Interface Anal.* **1999**, *27*, 629. (b) Gong, D.; Grimes, C. A.; Varghese, O. K.; Hu, W. C.; Singh, R. S.; Chen, Z.; Dickey, E. C. *J. Mater. Res.* **2001**, *16*, 3331.
(25) Shankar, K.; Mor, G. K.; Fitzgerald, A.; Grimes, C. A. *J. Phys. Chem. C* **2007**, *111*, 21.
(26) Varghese, O. K.; Gong, D. W.; Paulose, M.; Grimes, C. A.; Dickey, E. C. *J. Mater. Res.* **2003**, *18*, 156.
(27) Macak, J. M.; Tsuchiya, H.; Schmuki, P. *Angew. Chem., Int. Ed.* **2005**, *44*, 2100.
(28) Mor, G. K.; Varghese, O. K.; Paulose, M.; Shankar, K.; Grimes, C. A. *Sol. Energy Mater. Sol. Cells* **2006**, *90*, 2011.
(29) Park, J. H.; Kim, S.; Bard, A. J. *Nano Lett.* **2006**, *6*, 24.
(30) Macak, J. M.; Zlamal, M.; Krysa, J.; Schmuki, P. *Small* **2007**, *3*, 300.
(31) Albu, S. P.; Ghicov, A.; Macak, J. M.; Hahn, R.; Schmuki, P. *Nano Lett.* **2007**, *7*, 1286.
(32) Xu, Z. H.; Yu, J. G. *Nanotechnology* **2010**, *21*, 245501.
(33) Liang, H. C.; Li, X. Z. *Appl. Catal., B* **2009**, *86*, 8.
(34) Sohn, Y. S.; Smith, Y. R.; Misra, M.; Subramanian, V. *Appl. Catal., B* **2008**, *84*, 372.
(35) Albu, S. P.; Ghicov, A.; Aldabergenova, S.; Drechsel, P.; LeClere, D.; Thompson, G. E.; Macak, J. M.; Schmuki, P. *Adv. Mater.* **2008**, *20*, 4135.
(36) Macak, J. M.; Schmuki, P. *Electrochim. Acta* **2006**, *52*, 1258.
(37) Yu, J. G.; Dai, G. P.; Huang, B. B. *J. Phys. Chem C* **2009**, *113*, 16394.
(38) Yu, J. G.; Zhao, X. J. *Mater. Res. Bull.* **2001**, *36*, 97.
(39) Yu, J. C.; Ho, W. K.; Yu, J. G.; Hark, S. K.; Iu, K. *Langmuir* **2003**, *19*, 3889.
(40) Yu, J. G.; Wang, B. *Appl. Catal., B* **2010**, *94*, 295.
(41) Kang, S. H.; Kim, J.; Kim, H. S.; Sung, Y. *J. Ind. Eng. Chem.* **2008**, *14*, 52.
(42) Ishibashi, K.; Fujishima, A.; Watanabe, T.; Hashimoto, K. *Electrochem. Commun.* **2000**, *2*, 207.
(43) (a) Song, Y. Y.; Roy, P.; Paramasivam, I.; Schmuki, P. *Angew. Chem., Int. Ed.* **2010**, *49*, 351. (b) Xiao, Q.; Si, Z. C.; Zhang, J.; Xiao, C.; Tan, X. K. *J. Hazard. Mater.* **2008**, *150*, 62.
(44) Cheng, B.; Le, Y.; Yu, J. G. *J. Hazard. Mater.* **2010**, *177*, 971.
(45) Yu, J. G.; Wang, G. H.; Cheng, B.; Zhou, M. H. *Appl. Catal., B* **2007**, *69*, 171.
(46) Yu, J. C.; Yu, J. G.; Ho, W. K.; Jiang, Z. T.; Zhang, L. Z. *Chem. Mater.* **2002**, *14*, 3808.
(47) Lu, C. H.; Wu, W. H. *Mater. Sci. Eng., B* **2004**, *113*, 42.
(48) Yu, J. G.; Wang, W. G.; Cheng, B.; Su, B. L. *J. Phys. Chem. C* **2009**, *113*, 6743.
(49) (a) Dachille, F.; Simons, P. Y.; Roy, R. *Am. Mineral.* **1968**, *53*, 1929. (b) Matthews, A. *Am. Mineral.* **1976**, *61*, 419.
(50) (a) Yanagisawa, K.; Yamamoto, Y.; Feng, Q.; Yamasaki, N. *J. Mater. Res.* **1998**, *13*, 825. (b) Yanagisawa, K.; Ovenstone, J. *J. Phys. Chem. B* **1999**, *103*, 7781.
(51) Zhang, H. Z.; Banfield, J. F. *J. Mater. Res.* **2000**, *15*, 437.
(52) Yu, J. G.; Zhang, J. *Dalton Trans.* **2010**, *39*, 5860.
(53) (a) Albu, S P.; Ghicov, A.; Aldabergenova, S.; Drechsel, P.; LeClere, D.; Thompson, G. E.; Macak, J. M.; Schmuki, P. *Adv. Mater.* **2008**, *20*, 4135. (b) Park, H.; Choi, W. *J. Phys. Chem. B* **2004**, *108*, 4086.
(54) Li, D.; Haneda, H.; Hishita, S.; Ohashi, N. *Chem. Mater.* **2005**, *17*, 2588.
(55) Ohtani, B.; Ogawa, Y.; Nishimoto, S. *J. Phys. Chem. B* **1997**, *101*, 3746.
(56) Liu, Z. Y.; Zhang, X. T.; Nishimoto, S.; Jin, M.; Tryk, D. A.; Murakami, T.; Fujishima, A. *J. Phys. Chem. C* **2008**, *112*, 253.

JP106324X